Noncollinear Korringa-Kohn-Rostoker Green function method: Application to 3*d* nanostructures on Ni(001)

S. Lounis,* Ph. Mavropoulos,† P. H. Dederichs, and S. Blügel

Institut für Festkörperforschung, Forschungszentrum Jülich, D-52425 Jülich, Germany
(Received 29 September 2005; published 30 December 2005)

Magnetic nanostructures on nonmagnetic or magnetic substrates have attracted strong attention due to the development of interesting experimental methods with atomic resolution. Motivated by this progress we have extended the full-potential Korringa-Kohn-Rostoker Green-function method to treat noncollinear magnetic nanostructures on surfaces. We focus on magnetic 3*d* impurity nanoclusters, sitting as adatoms on or in the first surface layer on Ni(001), and investigate the size and orientation of the local moments and, moreover, the stabilization of noncollinear magnetic solutions. While clusters of Fe, Co, Ni atoms are magnetically collinear, noncollinear magnetic coupling is expected for Cr and Mn clusters on surfaces of elemental ferromagnets. The origin of frustration is the competition of the antiferromagnetic exchange coupling among the Cr or Mn atoms with the antiferromagnetic (for Cr) or ferromagnetic (for Mn) exchange coupling between the impurities and the substrate. We find that Cr and Mn first-neighboring dimers and a Mn trimer on Ni(001) show noncollinear behavior nearly degenerate with the most stable collinear configuration. Increasing the distance between the dimer atoms leads to a collinear behavior, similar to the one of the single impurities. Finally, we compare some of the noncollinear *ab initio* results to those obtained within a classical Heisenberg model, where the exchange constants are fitted to total energies of the collinear states; the agreement is surprisingly good.

I. INTRODUCTION

Theoretically, extensive work is carried out in the area of complex noncollinear magnetism, particularly for surface and bulk systems. A lot of interesting physics would be missed if only collinear magnetic structures were considered. In fact, magnetic nanostructures on magnetic or nonmagnetic substrates are attractive to the scientific community due to their unusual properties[1–4] being of relevance both for theory as well as for the applications in the magnetoelectronics devices.

One of these properties is the noncollinear magnetic order occurring for geometrically frustrated antiferromagnets, e.g., on a triangular lattice, in disordered systems, exchange bias systems, and molecular magnets, or for systems which exhibit either competing exchange interactions, or between exchange and spin-orbit interactions. A simple model for frustration is the following: Starting with an antiferromagnetic (AF) Cr dimer, the addition of a third Cr atom to form an equilateral triangle leads to a frustrated geometry. Each atom would like to couple antiferromagnetically to both other atoms. Since this is impossible, the moments of the three atoms rotate until a compromise is found. The ground state is then noncollinear, characterized by an angle of 120° between each atom. The same situation will also occur for the AF Cr dimer, since the interaction of both Cr atoms with the ferromagnetic substrate atoms is either ferromagnetic of antiferromagnetic. As we will show in this paper, also in this case a noncollinear structure can result.

The majority of the *ab initio* methods available for the treatment of noncollinear magnetism make explicit use of Bloch's theorem and are thus restricted to periodic systems (bulk or films). Then, even for collinear magnetism, one needs huge supercells to simulate impurities in a given host (bulk or film) in order to avoid spurious interactions of the impurities from adjacent supercells. A few methods have been developed to treat free clusters, but to our knowledge no *ab initio* methods exist for the investigation of noncollinear magnetism of clusters in bulk or deposited on surfaces.

First noncollinear calculations by the Korringa-Kohn-Rostoker (KKR) Green-function method, though not self-consistent, were already performed in 1985. Oswald *et al.*[5] could show by using the method of constraints that the exchange interaction between the moments of Mn and Fe impurity pairs in Cu is in good approximation described by the cos θ dependence of the Heisenberg model.

Sandratskii *et al.*[6] and Kübler and co-workers[7,8] pioneered the investigation of noncollinear magnetic structures using self-consistent density-functional theory. One of the first systems studied by Sandratskii *et al.*[6] was the spin spiral of bcc Fe with the KKR method. Later on, Δ-Fe was a hot topic, and the appearance of the experimental work of Tsunoda and co-workers[9,10] led to the development of other first-principles methods able to deal with noncollinear magnetism such as linear muffin-tin orbital,[11] ASW,[12] and FLAPW.[13–15]

Several papers[16,17] describe how symmetry simplifies the calculational effort for the spiral magnetic structures in the case of perfect periodic systems—this involves the generalized Bloch theorem. In *ab initio* methods, this principle is used together with the constrained density-functional theory[18,19] giving the opportunity of studying arbitrary magnetic configurations where the orientations of the local moments are constrained to nonequilibrium directions.

Concerning free clusters, few methods are developed. For example, Oda *et al.*[20] developed a plane-wave pseudopotential scheme for noncollinear magnetic structures. They applied it to small Fe clusters for which they found noncollinear magnetic structures for Fe_5 and linear-shape Fe_3. This

last result was in contradiction with the work of Hobbs *et al.*[21] who found only a collinear ferromagnetic configuration using a projector augmented-wave method. Small Cr clusters were found magnetically noncollinear,[20] as shown also by Kohl and Bertsch[22] using a relativistic nonlocal pseudopotential method after optimization of the ionic structure by a Monte Carlo technique. However, within the generalized gradient approximation (GGA) of density-functional theory, Hobbs *et al.*[21] find that in many cases the noncollinear states can be metastable, while the ground-state solutions are collinear and arise after geometrical optimization of the free-standing clusters.

One main result of Oda *et al.*[20] and Hobbs *et al.*[21] concerns the variation of the magnetization density with the position. The spin direction changes in the interstitial region between the atoms where the charge and magnetization densities are small, while the magnetization is practically collinear within the atomic spheres. This supports the use of a single spin direction for each atomic sphere as an approximation in order to accelerate the computation; this approximation is followed also here.

The aim of this work is to present a method based on the full-potential KKR scheme[23] which can deal with noncollinear magnetism in systems of reduced symmetry. This method is ideal for treating impurities or small clusters on surfaces or in bulk. As an application we study small $3d$ clusters on the Ni(001) surface where we find complex magnetic configurations.

II. NONCOLLINEAR KKR FORMALISM

The KKR method uses multiple-scattering theory in order to determine the one-electron Green function in a mixed site and angular-momentum representation. The retarded Green function is expanded as

$$G(\vec{R}_n + \vec{r}, \vec{R}_{n'} + \vec{r}';E) = -i\sqrt{E}\sum_L R_L^n(\vec{r}_<;E)H_L^n(\vec{r}_>;E)\delta_{nn'}$$
$$+ \sum_{LL'} R_L^n(\vec{r};E)G_{LL'}^{nn'}(E)R_{L'}^{n'}(\vec{r}';E).$$

$$(1)$$

Here, E is the energy and $\vec{R}_n$, $\vec{R}_{n'}$ refer to the atomic nuclei positions. By $\vec{r}_<$ and $\vec{r}_>$ we denote, respectively, the shorter and longer of the vectors $\vec{r}$ and $\vec{r}'$ which define the position in each Wigner-Seitz cell relative to the position $\vec{R}_n$ or $\vec{R}_{n'}$. The wave functions $R_L^n(\vec{r};E)$ and $H_L^n(\vec{r};E)$ are, respectively, the regular and irregular solutions of the Schrödinger equation for the potential V_n at site n, being embedded in free space; $L=(l,m)$ is a combined index for angular momentum quantum numbers; l is truncated at a maximum value of $l_{\max}$. The first term on the left-hand side of Eq. (1) is the so-called *single-site scattering term*, which describes the behavior of an atom n in free space. All multiple- and back-scattering information is contained in the second *back-scattering* term via the structural Green functions $G_{LL'}^{nn'}(E)$ which are obtained by solving the algebraic Dyson equation:

$$G_{LL'}^{nn'}(E) = \mathring{G}_{LL'}^{nn'}(E) + \sum_{n'',L''L'''} \mathring{G}_{LL''}^{nn''}(E)\Delta t_{L''L'''}^{n''}(E)G_{L'''L'}^{n''n'}(E).$$

$$(2)$$

Equation (2) follows directly from the usual Dyson equation of the form $G=\mathring{G}+\mathring{G}\Delta VG$, with ΔV the perturbation in the potential and $\mathring{G}$ the reference system Green function. The summation in Eq. (2) is over all lattice sites n'' and angular momenta L'' for which the perturbation $\Delta t_{L''L'''}^{n''}(E)=t_{L''L'''}^{n''}(E)-\mathring{t}_{L''L'''}^{n''}(E)$ between the t matrices of the real and the reference system is significant (the t matrix gives the scattering amplitude of the atomic potential). The quantities $\mathring{G}_{LL'}^{nn'}(E)$ are the structural Green functions of the reference system. For the calculation of a crystal bulk or surface, the reference system can be free space, or, within the tight-binding KKR formulation,[24] a system of periodically arrayed repulsive potentials. After the host (bulk or surface) Green function is found, it can be used in a second step as a reference for the calculation of the Green function of an impurity or a cluster of impurities embedded in the host.

The algebraic Dyson equation (2) is solved by matrix inversion, as we will see later on in Eq. (17). In the case of spin-dependent electronic structure, spin indexes enter in the t matrix, the Green functions and in Eq. (2). Especially in the case of noncollinear magnetism, these quantities become 2 $\times$ 2 matrices in spin space, denoted by t and G.

Once the spin-dependent Green function is known, all physical properties can be derived from it. In particular, the charge density $n(\vec{r})$ and spin density $\vec{m}(\vec{r})$ are given by an integration of the imaginary part of G up to the Fermi level E_F and a trace over spin indexes s (putting the Green function in a matrix form in spin space):

$$n(\vec{r}) = -\frac{1}{\pi}\text{Im Tr}_s \int^{E_F} G(\vec{r},\vec{r};E)dE, \qquad (3)$$

$$\vec{m}(\vec{r}) = -\frac{1}{\pi}\text{Im Tr}_s \int^{E_F} \vec{\sigma}G(\vec{r},\vec{r};E)dE. \qquad (4)$$

Here, $\vec{\sigma}=(\sigma_x,\sigma_y,\sigma_z)$ are the Pauli matrices and Tr_s means the trace operation in spin space.

The basic difference between noncollinear and collinear magnetism is the absence of a natural spin-quantization axis common to the whole crystal. The density matrix is not anymore diagonal in spin space as in the case of collinear magnetism. Instead, in any fixed frame of reference it has the form

$$\boldsymbol{\rho}(\vec{r}) = \begin{bmatrix} \rho_{\uparrow\uparrow}(\vec{r}) & \rho_{\uparrow\downarrow}(\vec{r}) \\ \rho_{\downarrow\uparrow}(\vec{r}) & \rho_{\downarrow\downarrow}(\vec{r}) \end{bmatrix} = \frac{1}{2}[n(\vec{r}) + \vec{\sigma}\cdot\vec{m}(\vec{r})]. \qquad (5)$$

At any *particular point* in space, of course, a *local* frame of reference can be found in which $\boldsymbol{\rho}$ is diagonal, but this local frame can change from point to point.

In order to deal with noncollinear magnetism, we have to solve the appropriate Dyson equation. First we define the reference system which is a perfect surface characterized by collinear magnetism. Although the collinearity of the refer-

ence system is not a necessary requirement, it serves our purpose of calculating the electronic structure of the ferromagnetic or nonmagnetic surfaces which are used as reference systems. Thus the host Green functions $\mathring{G}$ and t matrices $\mathring{t}$ are assumed diagonal in spin space. In this way, in the case of a magnetic host, a global spin frame of reference is defined. The host $\mathring{G}$ and $\mathring{t}$ are thus of the form

$$\mathring{G}(E) = \begin{bmatrix} \mathring{G}_{\uparrow\uparrow}(E) & 0 \\ 0 & \mathring{G}_{\downarrow\downarrow}(E) \end{bmatrix}; \quad \mathring{t}(E) = \begin{bmatrix} \mathring{t}_{\uparrow\uparrow}(E) & 0 \\ 0 & \mathring{t}_{\downarrow\downarrow}(E) \end{bmatrix}. \quad (6)$$

Then the perturbed system is constructed. The impurity atoms which might couple magnetically in a noncollinear way reside on the surface, perturbing the potential at a few neighboring sites (atoms or empty cells representing the potential in the vacuum). Within this finite cluster of perturbed sites the magnetization can be noncollinear leading to the appearance of nondiagonal elements of the t matrix:

$$t(E) = \begin{bmatrix} t_{\uparrow\uparrow}(E) & t_{\uparrow\downarrow}(E) \\ t_{\downarrow\uparrow}(E) & t_{\downarrow\downarrow}(E) \end{bmatrix}. \quad (7)$$

The nondiagonal t matrix contains the information on spin-flip scattering by the atomic potential.

At this stage an approximation enters our method. It is assumed that, separately for each atom, there exists an intra-atomic spin-quantization axis common to the whole atomic cell. This axis is identified with the spatial average of the magnetization density $\vec{m}_n(\vec{r})$ in each cell n. This defines the local spin frame of reference. In this way we neglect the variation of the spin-quantization axis within the cell during self-consistency, avoiding the time-consuming numerical solution of the potential of coupled Schrödinger equations of the two spin channels. Within the local-density approximation of density-functional theory, the exchange correlation potential has the same reference frame as the local magnetization $\vec{m}_n(\vec{r})$. Then for each atom we have a potential which is collinear in the local frame, and the solutions of the Schrödinger equation, $R^{loc}_{nLs}(\vec{r};E)$ and $H^{loc}_{nLs}(\vec{r};E)$, depending on the spin index s of the local frame.

The solution of the Schrödinger equation separately for each spin channel provides also the diagonal t matrix of each atomic cell n in the local frame of reference:

$$t^{loc}_n(E) = \begin{bmatrix} t^{loc}_{\uparrow\uparrow}(E) & 0 \\ 0 & t^{loc}_{\downarrow\downarrow}(E) \end{bmatrix}. \quad (8)$$

Then the t matrix is rotated from the local to the global spin frame of reference using the spin rotation matrix U_n:

$$t^{glob}_n(E) = U_n t^{loc}_n(E) U^\dagger_n, \quad (9)$$

U_n being given by

$$U_n = \begin{bmatrix} \cos\left(\dfrac{\theta_n}{2}\right)e^{-(i/2)\phi_n} & -\sin\left(\dfrac{\theta_n}{2}\right)e^{-(i/2)\phi_n} \\ \sin\left(\dfrac{\theta_n}{2}\right)e^{(i/2)\phi_n} & \cos\left(\dfrac{\theta_n}{2}\right)e^{(i/2)\phi_n} \end{bmatrix}. \quad (10)$$

The polar angles θ_n and ϕ_n define the direction of the local magnetic moment with respect to the global spin frame of reference. Normally, θ_n and ϕ_n vary within the atomic cell, but in the approximation used here, average angles are defined for each cell via an averaging of the magnetization density within the cell. Of course, when self-consistency is achieved, both the averaged and the point-by-point varying magnetization direction can be extracted from the output density matrix. Thus the assumption of a unique spin direction in each cell is only made for the spin-dependent potential.

The t matrix in the global spin frame of reference can be rewritten in the following way:

$$t^{glob}_n(E) = U_n\left(\frac{1}{2}[t^{loc}_{\uparrow\uparrow}(E) + t^{loc}_{\downarrow\downarrow}(E)]\mathbf{1} + \frac{1}{2}[t^{loc}_{\uparrow\uparrow}(E) - t^{loc}_{\downarrow\downarrow}(E)]\boldsymbol{\sigma}_z\right)U^\dagger_n \quad (11)$$

with $\boldsymbol{\sigma}_z$ the z component of the Pauli matrices:

$$\boldsymbol{\sigma}_z = \begin{bmatrix} 1 & 0 \\ 0 & -1 \end{bmatrix}. \quad (12)$$

It is convenient to define the projection matrices $\boldsymbol{\sigma}_{ns}$ for the local spin-up ($\uparrow$) and spin-down ($\downarrow$) directions as

$$\boldsymbol{\sigma}_{ns} = \frac{1}{2}U_n(\mathbf{1} \pm \boldsymbol{\sigma}_z)U^\dagger_n = (\boldsymbol{\sigma}_{ns})^2 \quad (+ \text{ for } s=\uparrow, \ - \text{ for } s=\downarrow). \quad (13)$$

Then $t^{glob}_n(E)$ is written as

$$t^{glob}_n(E) = t^{loc}_{n\uparrow\uparrow}(E)\boldsymbol{\sigma}_{n\uparrow} + t^{loc}_{n\downarrow\downarrow}(E)\boldsymbol{\sigma}_{n\downarrow}. \quad (14)$$

In the collinear case the local and global frames are identical and the projection operators reduce to

$$\boldsymbol{\sigma}_\uparrow = \begin{bmatrix} 1 & 0 \\ 0 & 0 \end{bmatrix}, \quad \boldsymbol{\sigma}_\downarrow = \begin{bmatrix} 0 & 0 \\ 0 & 1 \end{bmatrix} \quad \text{(collinear case)}. \quad (15)$$

At this stage, the difference between the t matrices $\Delta t^{glob}_n = t^{glob}_n - \mathring{t}_n$ is calculated in order to get all the ingredients to solve the Dyson equation for the structural Green function [$\mathring{t}_n$ has been defined in the global frame in Eq. (6)]. This is the analog of Eq. (2) in matrix form in spin space:

$$G_{str}(E) = \mathring{G}_{str}(E) + \mathring{G}_{str}(E)\Delta t^{glob}(E)G_{str}(E). \quad (16)$$

Here, in analogy to Eq. (1) and Eq. (2), $G_{str}(E)$ are matrices of size 2×2 in spin space, size $(l_{max}+1)^2 \times (l_{max}+1)^2$ in angular momentum space, and size $N\times N$ (with N the number of sites) in real space; all these indices are combined to form $2\times(l_{max}+1)^2\times N$-dimensional matrices. The t matrix itself is diagonal in real-space site indexes. The solution of Eq. (16)

for the structural Green function requires matrix inversion, yielding $\boldsymbol{G}_{\mathrm{str}}(E)$ in the global frame:

$$\boldsymbol{G}_{\mathrm{str}}(E) = \overset{\circ}{\boldsymbol{G}}_{\mathrm{str}}(E)[1 - \Delta t^{\mathrm{glob}}(E)\overset{\circ}{\boldsymbol{G}}_{\mathrm{str}}(E)]^{-1}. \quad (17)$$

Equation (1) can be now rewritten in the noncollinear case in order to obtain the Green function in the global frame. Using the matrices $\boldsymbol{\sigma}_{ns}$ [Eq. (13)] to project the local wave functions to the global frame, the Green function is written as

$$\begin{aligned}
\boldsymbol{G}^{\mathrm{glob}}(\vec{R}_n + \vec{r}, \vec{R}_{n'} + \vec{r}'; E) \\
= -i\sqrt{E} \sum_{Ls} R^{\mathrm{loc}}_{nLs}(\vec{r}_<; E) H^{\mathrm{loc}}_{nLs}(\vec{r}_>; E) \boldsymbol{\sigma}_{ns} \\
+ \sum_{LL'ss'} R^{\mathrm{loc}}_{nLs}(\vec{r}; E) \boldsymbol{\sigma}_{ns} \boldsymbol{G}^{\mathrm{glob}}_{LL'nn'}(E) \boldsymbol{\sigma}_{n's'} R^{\mathrm{loc}}_{n'L's'}(\vec{r}'; E). \quad (18)
\end{aligned}$$

If needed, the Green function can be rotated to the local frame of any atom by the use of the transformation matrices U_n [Eq. (10)]. We point out that, even in the local frame of reference, the Green function is not in general diagonal in spin space. Finally we calculate the charge density and spin density from Eqs. (3) and (4). The spin-dependent local density of states within the Wigner-Seitz cell (WS) of each site n is

$$n_{ns}(E) = -\frac{1}{\pi} \int_{\mathrm{WS}} \mathrm{Im}\, G_{ss}(\vec{R}_n + \vec{r}, \vec{R}_n + \vec{r}; E) d^3r. \quad (19)$$

The spin density $\vec{m} = (m^x, m^y, m^z)$ [Eq. (4)] is noncollinear. The new polar angles at each site n can then be obtained for each point by

$$\tan \theta_n(\vec{r}) = \frac{m^z_n(\vec{r})}{m_n(\vec{r})}, \quad \tan \phi_n(\vec{r}) = \frac{m^y_n(\vec{r})}{m^x_n(\vec{r})} \quad (20)$$

or as an average over the local Wigner-Seitz cell

$$\tan \theta_n = \frac{\int_{\mathrm{WS}} m^z_n(\vec{r}) d\vec{r}}{\int_{\mathrm{WS}} m_n(\vec{r}) d\vec{r}}, \quad \tan \phi_n = \frac{\int_{\mathrm{WS}} m^y_n(\vec{r}) d\vec{r}}{\int_{\mathrm{WS}} m^x_n(\vec{r}) d\vec{r}}. \quad (21)$$

III. APPLICATIONS

As an application of our method, we study the magnetic state of $3d$-atom clusters in and on the Ni(001) surface. In a first step, we study the adatom properties, which are already known from previous work. In a second step, we perform calculations for $3d$ dimers and trimers and use the understanding gained from the single adatoms in order to explain the results.

Our calculations henceforth are based on the local-spin-density approximation (LSDA) of density-functional theory with the parametrization of Vosko *et al.*[32] The full nonspherical potential was used, taking into account the correct description of the Wigner-Seitz atomic cells.[33] Angular mo-

menta up to $l_{\max} = 3$ were included in the expansion of the Green functions and up to $2l_{\max} = 6$ in the charge-density expansion. Relativistic effects were described in the scalar relativistic approximation.

First, the surface Green functions are determined by the screened KKR method[24] for the (001) surface of Ni which serves as the reference system. The equilibrium lattice parameter of Ni was used (6.46 a.u. ≈ 3.42 Å). To describe the impurities on the surface (later we refer to these as *adatoms* and to the impurities sitting in the first surface layer as *inatoms*), we consider a cluster of perturbed potentials which includes the potentials of the impurities and the perturbed potentials of several neighboring shells, with typical size ranging from 19 perturbed sites for the single impurity to 32 for the dimers and trimers; in all cases, at least the first neighboring sites of the impurity atoms were taken into account in the calculation to ensure the correct screening of the impurity potential. Test calculations have shown that this is adequate for our work; this is a merit of the Green-function method, in which the correct boundary conditions of the host (in our case of the host surface) are included in the Green function via the Dyson equation. We consider the adatoms at the unrelaxed hollow position in the first vacuum layer, and the inatoms at the unrelaxed position in the first surface layer.

The orientations assigned to the spin moments of the impurities are always relative to the orientation of the substrate moment, which we take as the global frame. This, in turn, depends on delicate physical quantities such as the magnetic anisotropy energy, which cannot be related to the local properties of the small clusters that we study. In the present approach such effects arising from spin-orbit interaction are not included. The direction of the host moments must therefore be considered as an input parameter from experiments or from independent *ab initio* calculations.

A. 3d single adatoms and inatoms

$3d$ adatoms on Fe(001) and on Ni(001) have been already studied previously, using the KKR method[25–28] in the atomic sphere approximation. Here we repeat the calculations of $3d$ adatoms on Ni(001) using the full potential method [a detailed work on Fe and Co on Ni(001) is presented in a recent article[29]]. We give a brief analysis of the results, which are basically unchanged, in order to use them as a step for understanding the behavior of dimers and trimers later on.

A collinear calculation of the magnetic state of a single adatom on a ferromagnetic substrate can give in some cases two solutions: one with ferromagnetic (FM) coupling to the substrate and one with antiferromagnetic (AF) coupling. One of these states will correspond to the real ground state, and the other to a local minimum; this is actually a local minimum with respect to collinear variations of the magnetic moment, since the angle θ between the local moment and the substrate moment cannot be varied in a collinear calculation. From total-energy calculations of the two states, the ground state can be then determined. In some cases, when the intra-atomic exchange field is not strong (beginning or end of the $3d$ series), only one of the two minima exists. On the other
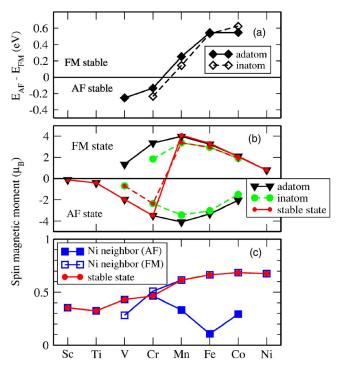
FIG. 1. (Color online) 3*d* adatoms and inatoms on Ni(001): (a) Energy difference between the AF and FM coupling, the values related to adatom and inatoms are described by, respectively, full and empty black diamonds; (b) magnetic moments of the adatoms (triangles) and inatoms (circles) within the two possible magnetic configurations FM and AF; (c) the variation of the magnetic moments of Ni first nearest neighbors of the adatoms.

hand, if noncollinear effects are included in the calculations, one of the two minima usually becomes unstable against an angular rotation of the moment, i.e., it is then actually a saddle point.

The full diamonds in Fig. 1(a) show the energy difference between the AF and the FM solution for 3*d* adatoms on Ni(001). The first elements of the 3*d* series (Sc, Ti, V, Cr) are AF coupled to the substrate whereas the coupling of Mn, Fe, Co, and Ni is FM. Sc (AF), Ti (AF), and Ni (FM) are characterized by a single solution. Clearly, the AF-FM transition occurs when the adatom atomic number changes from Cr ($Z=24$) to Mn ($Z=25$). This transition can be interpreted as in the case of the interatomic interaction of magnetic

dimers,[30,31] in terms of the energy gain due to the formation of hybrid states with the Ni substrate as the 3*d* virtual bound state comes lower in energy with increasing Z. An explanation (see Fig. 2) can be given in terms of the $d-d$ hybridization between the adatom 3*d* states and the Ni substrate 3*d* states. Energy is gained when a half-occupied d virtual bound state (VBS) at E_F is broadened by hybridization with the Ni minority 3*d* states, which lie at E_F (the Ni majority d states are fully occupied and positioned below E_F). For the early 3*d* adatoms [Fig. 2(a)], it is the majority d VBS which is at E_F, thus the majority-spin direction of the adatom is favorably aligned with the minority-spin direction of Ni, and an AF coupling arises. For the late 3*d* adatoms [Fig. 2(b)], on the contrary, the minority d VBS is at E_F, and this aligns with the Ni minority d states; then a FM coupling arises. For our purposes we keep in mind that, since Cr and Mn are in the intermediate region, i.e., near the AF-FM transition point, their magnetic coupling to the Ni substrate is weak; this has consequences to be seen in the behavior of dimers, trimers, etc., in the next subsections.

The magnetic moments of the adatoms and Ni first neighbors in the surface layer are shown in Figs. 1(b) and 1(c). Evidently the moment of the Ni first neighbors is strongly affected by the adatoms. Especially in the AF state for Mn, Fe, and Co adatoms, the Ni moment is strongly reduced and the FM configuration is stable. As regards the adatom moments, due to its half filled d band the Mn adatom carries the highest magnetic moment ($4.09\mu_B$) followed by Cr ($3.48\mu_B$) and Fe ($3.24\mu_B$).

To understand the effect of coordination and stronger hybridization on the magnetic behavior of the adatoms, we take the case of impurities sitting in the first surface layer (inatoms). We carried out the calculations for V, Cr, Mn, Fe, and Co impurities. The corresponding spin moments are shown in Fig. 1(b) (circles), and the FM-AF energy differences are shown in Fig. 1(a) (open diamonds and dashed line).

Compared to the adatom case, the spin moments are reduced, especially for V and Cr. This effect is expected due to the increase of the coordination number from 4 to 8 and the subsequent stronger hybridization of the 3*d* levels with the host wave functions. Moreover, the energy difference ΔE between the AF and FM solutions is affected. The trend can be understood as follows. In the case of Cr, the reduction of the local magnetic moment M is accompanied by a reduction of the exchange splitting ΔE_X as $\Delta E_X \approx IM$, where $I \approx 1$ eV
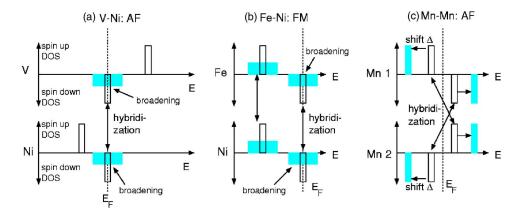

FIG. 2. (Color online) Alexander-Anderson model for neighboring magnetic atoms: (a) early 3*d* transition elements in interaction with Ni surface atoms; (b) late 3*d* transition elements in interaction with Ni surface atoms; (c) Cr or Mn dimer.
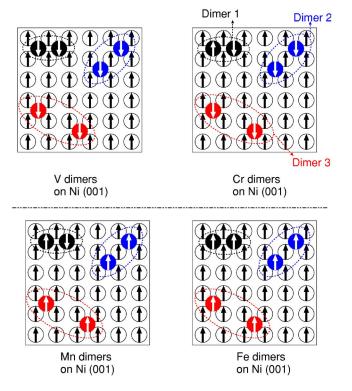
FIG. 3. (Color online) Different geometrical configurations considered for dimers at the surface of Ni(001). Dimer-1 type corresponds to the case where the atoms are first neighboring atoms, dimer-2 type where the atoms are 2′NN and finally dimer-3 type to 4′NN. The collinear magnetic ground states are also shown for V, Cr, Mn, and Fe dimers.

is the intra-atomic exchange integral. This means that, for the inatom, the occupied 3d states are closer to E_F than for the adatom. In turn, this intensifies the hybridization of these states with the Ni 3d states (which are close to E_F). At the same time, also the higher coordination number intensifies the d-d hybridization. The hybridization-induced level shift in the AF configuration increases, and the energy of the AF state is thus lowered. The same mechanism is responsible for the weakening of the FM coupling of Mn inatom compared to the adatom. Similarly, the stronger hybridization of the Co-inatom d states stabilizes even more its FM configuration due to the energy gain from the broadening of the d virtual bound state.

B. Adatom and inatom dimers

Having established the single adatom behavior, we turn to adatom dimers. We considered three geometries of increas-

ing distance: dimers as first, second, and fourth neighbors. We will discuss the magnetic interaction between the dimer atoms and the resulting magnetic order, first looking only at collinear states and then allowing for noncollinear order. We will see how, in certain cases, the collinear state reduces the symmetry, while the noncollinear state restores the full symmetry of the system. Noncollinear order is finally established for certain first-neighbor dimers.
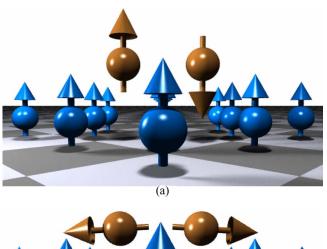
Figure 3 represents schematically the different considered geometrical configurations of impurity dimers residing on the surface. We have investigated the dimer-1 type of geometry (the adatoms are first neighboring atoms), dimer-2 type (the adatoms are second neighbors), and dimer-3 type (the adatoms are fourth neighbors). This allows us to monitor the strength of the magnetic coupling as a function of the distance. Three collinear magnetic configurations were treated: (i) antiferromagnetic coupling within the dimer leading to a ferrimagnetic solution (Ferri), (ii) ferromagnetic coupling within the dimer with both atoms ferromagnetically coupled to the substrate (FM), or (iii) ferromagnetic coupling within the dimer with both atoms antiferromagnetically coupled to the substrate (AF).
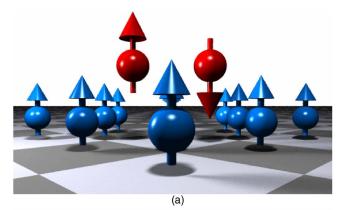
Our calculations include V, Cr, Mn, and Fe dimers. We found that all V and Fe dimer types behave like the adatoms: in all geometries, both V atoms are AF and both Fe atoms are FM. On the other hand, Cr and Mn dimers show magnetic frustration. As shown in Fig. 3, both the Cr dimer 1 and Mn dimer 1 show (in a collinear calculation) a Ferri ground state (see Table I). With increasing distance between the adatoms, a transition occurs to the single adatom magnetic behavior which is AF for Cr dimers and FM for Mn dimers. It is clear that, in the dimer-1 case, there is a competition of exchange interactions.

When we allow for a rotation of the magnetic moments, noncollinear solutions are obtained for the Cr and Mn dimer-1 systems. On the other hand, the magnetic coupling of the V and Fe dimer 1 remains collinear. Let us start with Cr dimer 1: Fig. 4(a) represents the collinear magnetic ground state. As one expects from the adatom picture, both adatoms forming the dimer tend to couple AF to the substrate but due to their half filled d band they also tend to couple AF to each other. This can be understood in terms of the Alexander-Anderson model[30,31]. To give a short explanation [see Fig. 2(c)], both Cr and Mn have their majority-spin VBS occupied, below E_F, and the minority-spin VBS unoccupied, above E_F. An antiparallel configuration between the moments in a Mn or Cr dimer lowers the energy, because the occupied d VBS of each atom hybridizes with the unoccupied d VBS of the other atom and is shifted to lower eigenvalues. Contrary to this, a parallel coupling does not lower

TABLE I. Energy differences between the Ferri solution and the FM (AF) configuration for the three types of dimers investigated.

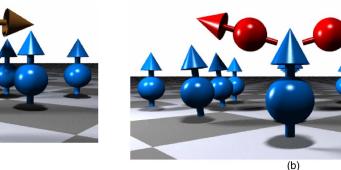|	Cr			Mn		
	Dimer 1	Dimer 2	Dimer 3	Dimer 1	Dimer 2	Dimer 3
$E_{FM}-E_{Ferri}$ (eV)	0.451	0.130	0.120	0.065	−0.242	−0.239
$E_{AF}-E_{Ferri}$ (eV)	0.433	−0.093	−0.112	0.496	0.187	0.233

(a)

(b)

FIG. 4. (Color online) Most stable configurations of Cr dimer-1 type obtained with (a) the collinear KKR method and (b) the noncollinear KKR method. The rotation angle with respect to the z axis is equal to $94.2°$. The collinear state is the ground state, with the noncollinear state being a local minimum (see text).

(a)

(b)

FIG. 5. (Color online) Most stable configurations of Mn dimer-1 type obtained with the collinear KKR method (a) and noncollinear KKR method (b). The rotation angle with respect to the z axis is equal to $72.6°$. The noncollinear state is the ground state.

the energy, since there is no level shifting, but only level broadening of the majority d VBS. Since these are fully occupied, the broadening brings no energy gain.

Thus there is a competition between the interatomic coupling within the dimer, which drives it to a Ferri state, and the exchange interaction with the substrate, which drives the moments of both atoms in the same direction: AF for Cr and FM for Mn. As discussed in the previous subsection, the magnetic exchange interaction (MEI) to the substrate is relatively weak for Cr and Mn. Thus the *intradimer* MEI is stronger than the MEI with the substrate, and in the collinear approximation the ground state is found ferrimagnetic (Ferri). Removing the collinear constraint, a compromise can be found such that both atoms are AF coupled to each other and at the same time (for Cr) slightly AF coupled to the substrate. This is shown in Fig. 4(b): the Cr adatom moments are aligned antiparallel to each other and basically perpendicular to the substrate moments. However, the weak AF interaction with the substrate causes a slight tilting towards the substrate, leading to an angle of $94.2°$ instead of $90°$. We also observe a very small tilting ($\approx 0.3°$) of the magnetic moments of the four outer Ni atoms neighboring the Cr dimer (the two inner Ni atoms do not tilt for symmetry reasons).

Despite the above considerations, the collinear Ferri state [Fig. 4(a)] is also a self-consistent solution of the Kohn-Sham equations, even if the collinear constraint is removed. Total-energy calculations are needed in order to determine if the noncollinear state is the true ground state, or if it represents a local minimum of energy with the collinear result representing the true ground state. After performing such calculations we find that the ground state is collinear with an energy difference of $\Delta E_{\text{Ncol-Ferri}} = 39.84$ meV (increasing the angular-momentum cutoff to $l_{\max}=4$ brought no significant change to this result).

The case is different for Mn dimers. Figure 5 shows the collinear and the noncollinear solutions. The dimer atoms couple strongly antiferromagnetically to each other but the single Mn adatoms tend to couple (weakly) ferromagnetically to the substrate. Both adatom moments, while aligned antiferromagnetically with respect to each other, are tilted in the direction of the substrate magnetization, as opposed to the Cr dimer. With a rotation angle of $\approx 72.6°$, the tilting from the $90°$ configuration is rather large. Also the Ni moments are tilted by $7.4°$. The main difference with the case of Cr dimer 1 is that for Mn dimer 1 the noncollinear solution is the ground state (total-energy calculations yield $\Delta E_{\text{Ncol-Ferri}} = -13.45$ meV). The spin moments of the V, Cr, Mn, and Fe dimers are given in Table III.

In both cases (Cr and Mn dimers) the frustrated collinear solution is asymmetric, while the noncollinear ground state restores the twofold symmetry of the system. The differences in energy between the Ferri and the noncollinear solutions are small and can be altered either by using a different type of exchange and correlation functional such as GGA or LSDA+U, or after relaxing the atoms. We note, however, that in a test calculation we found the Cr single-adatom relaxation to be small (3.23% inward with respect to the inter-

TABLE II. Values of magnetic exchange parameters J_{ij} for Cr and Mn dimers on Ni(001), fitted from collinear first-principles total-energy calculations (b) and obtained by the Lichtenstein formula (Ref. 34) (a) (J_{Cr-Ni} and J_{Mn-Ni} are averaged over the different Ni first neighbors of the dimer atoms). Positive J_{ij} correspond to ferromagnetic interactions, negative J_{ij} to antiferromagnetic ones.

| J_{ij} (meV) | (a) | (b) | | |
	Dimer 1	Dimer 1	Dimer 2	Dimer 3
J_{Cr-Ni}	−1.3	−11.6	−13.9	−14.5
J_{Cr-Cr}	−189.1	−221.3	−9.2	−2.0
J_{Mn-Ni}	13.0	27.0	26.8	29.5
J_{Mn-Mn}	−138.2	−140.2	13.7	1.5

layer distance), and thus we believe that the relaxation cannot affect the exchange interaction considerably.

As a cross check, it is interesting to compare these noncollinear *ab initio* results to model calculations based on the Heisenberg model with the exchange parameters fitted to the total-energy results. We assume a classical spin Hamiltonian of the form

$$H = -\frac{1}{2}\sum_{i \neq j} J_{ij}\vec{e}_i\vec{e}_j. \qquad (22)$$

Here, $\vec{e}$ is a unit vector defining the direction of the magnetic moment and i and j indicate the dimer atoms and their first Ni neighbors. We can evaluate the interatomic exchange constants J_{Cr-Ni}, J_{Mn-Ni}, J_{Mn-Mn}, and J_{Cr-Cr} via a fit to the total energy obtained from collinear LSDA calculations of the FM, AF, and Ferri configurations. Taking into account only first-neighbor interactions and neglecting the rotation of Ni moments, we rewrite the Hamiltonian for the dimer in terms of the tilting angles θ_1 and θ_2 of the two Cr (or Mn) atoms (the azimuthal angles ϕ do not enter the expression because of symmetry reasons):

$$H = -J_{Cr-Cr}\cos(\theta_1 - \theta_2) - 4J_{Cr-Ni}(\cos\theta_1 + \cos\theta_2) + \text{const.} \qquad (23)$$

We note the two extreme cases arising from this Heisenberg Hamiltonian: (i) $|J_{Cr-Ni}| \gg |J_{Cr-Cr}|$ leads to the stabilization of the collinear FM or AF configuration (adatomlike behavior) and (ii) $|J_{Cr-Ni}| \ll |J_{Cr-Cr}|$ leads to antiferromagnetic coupling within the dimer if $J_{Cr-Cr} < 0$. Within the Heisenberg model the Ferri solution and the noncollinear solution with $\theta=90°$ have the same energy.

Table II summarizes the estimated exchange parameters. Two effects are striking: (i) The strong antiferromagnetic Cr-Cr and Mn-Mn interaction for the dimer 1 (nearest neighbors), being an order of magnitude larger than the exchange interactions with the substrate and being responsible for the stabilization of the noncollinear state structures shown in Figs. 4 and 5. (ii) The very weak Cr-Cr and Mn-Mn interactions in the dimer-2 and -3 configurations. Whereas for the nearest-neighbors configuration (dimer-1) the direct overlap of the d-wave functions of the Cr and Mn atoms leads to the strong coupling, this overlap is missing for larger distances

and the interaction can only proceed through the substrate. However, this interaction is weak, in fact considerably smaller than the interaction of both adatoms with the four neighboring Ni atoms of the substrate. Therefore these dimers are effectively decoupled, and behave like the isolated adatoms, being antiferromagnetically coupled to the substrate in the case of Cr and ferromagnetically for Mn. The exchange constants J_{ij} fitted to total-energy results can be compared to the ones obtained by using the Lichtenstein formula (starting from the Ferri ground state). This rests on the force theorem, and yields the exchange constants relevant to an infinitesimal rotation of the moments. The results of the two methods agree best for the Mn-Mn interaction, and reasonably well for the Cr-Cr interaction, but not for Mn-Ni and Cr-Ni.

With the parameters from Table II one can also recalculate the noncollinear structure of the ground state. The agreement with the *ab initio* results is quite reasonable. For the Cr dimer, one finds a slightly smaller tilting, i.e., 96° instead of 94.2°, while for the Mn dimer the angle is 67.3° instead of 70.6°.

The differences in energy calculated within this simple model show that the Cr dimer 1 has a noncollinear ground state ($\Delta E_{Ncol-Ferri}=-9.7$ meV) as well as the Mn dimer 1 ($\Delta E_{Ncol-Ferri}=-41.6$ meV). The discrepancy obtained for the case of Cr dimer 1 (the LSDA calculation gives the collinear Ferri ground state) can be attributed to the restrictions of the Heisenberg model. For instance, for the Ferri and noncollinear configurations, the Cr moments are slightly different, and also the reduction of the Ni moments as a function of the rotation angle (e.g., for the single adatom) cannot be described by the Heisenberg model, where the absolute values of the moments are assumed to be constant. Within the Heisenberg model, the Ferri solution (with $\theta_1=0°$ and $\theta_2=180°$) is degenerate with the noncollinear solution ($\theta_{1,2}=90°$ with AF coupling within the dimer).

To evaluate the effect of change in coordination and hybridization, we have undertaken a study of inatom first-neighbor dimers for V, Cr, Mn, and Fe. The V and Fe inatom dimers were found to behave like the adatom dimers. The V dimer is in an AF state, the Fe dimer in a FM state, while the Cr and Mn dimers are in a Ferri state (in the case of collinear constraint). The spin moments in the collinear and noncollinear states are given in Table III. Within the Ferri dimers, the difference between the moments of the two atoms is due to the different kind of coupling that each inatom has with the substrate (AF or FM). One notices also that the magnetic moments in the ground state decrease compared to the values obtained for the single inatoms and single adatoms. When the rotation of the moments is allowed, Cr dimer can be stabilized at an angle of 107° (instead of 94.2° found for the adatom-dimer case), and Mn dimer at an angle of 80.9° (instead of 72.6°). Thus the noncollinear solutions obtained for inatom dimers are rather similar to what was obtained for adatom dimers. Energetically, however, both the Cr and the Mn inatom dimers show a lower total energy in the collinear Ferri state (for Cr, $\Delta E_{Ncol-Ferri}=24.11$ meV; for Mn, $\Delta E_{Ncol-Ferri}=22.5$ meV).

TABLE III. Atomic spin moments (in μ_B) of the adatom and inatom dimers (of type 1, i.e., nearest neighbors) in the collinear and noncollinear configurations. A minus sign of the collinear moments indicates an antiparallel orientation with respect to the substrate magnetization. Embedding the dimer into the surface causes, as expected, a decrease of the spin moments due to stronger hybridization of the d-wave functions.

Dimer type	V (AF)	Cr (Ferri)	Cr (Ncol)	Mn (Ferri)	Mn (Ncol)	Fe (FM)
On Ni(001)	$(-1.28, -1.28)$	$(-3.04, 3.05)$	$(3.03, 3.03)$	$(-3.84, 3.69)$	$(3.75, 3.75)$	$(3.10, 3.10)$
In Ni(001)	$(-0.32, -0.32)$	$(-2.00, 1.96)$	$(1.97, 1.97)$	$(-3.32, 3.20)$	$(3.26, 3.26)$	$(2.88, 2.88)$

C. Trimers

Following the same procedure as for dimers we first investigated several collinear magnetic configurations for the most compact trimer on the Ni(001) surface, which has the shape of an isosceles rectangular triangle (see Fig. 6) of side $\sqrt{2}a/2$ and hypotenuse a (a is the Ni fcc lattice constant). It is expected, and verified by total-energy calculations, to find the $\downarrow\uparrow\downarrow$ configuration as the collinear magnetic ground state for Cr and the $\uparrow\downarrow\uparrow$ for the Mn trimer ($\uparrow$ means an atomic
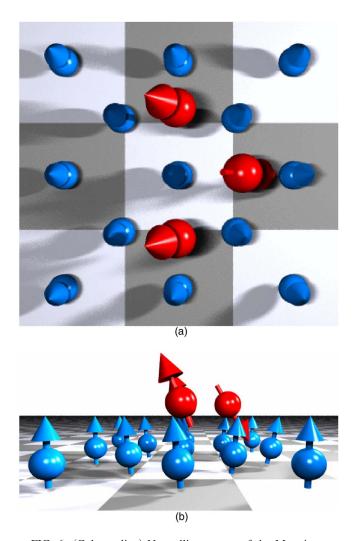

(a)

(b)

FIG. 6. (Color online) Noncollinear state of the Mn trimer on Ni(001) surface. Side view (a) and front view (b) are shown. This represents a local minimum in energy, with the collinear state being the ground state (see text).

moment parallel to the substrate, $\downarrow$ an antiparallel one; the middle arrow represents the direction of the atomic moment at the right-angle corner of the triangle). In Table IV, the energy differences among the possible collinear configurations are given; for the $\uparrow\uparrow\uparrow$ and $\downarrow\downarrow\downarrow$ Cr trimers, no self-consistent solution could be found.

Allowing free rotation of the magnetic moments leads to no change for the Cr trimer $\downarrow\uparrow\downarrow$—the state remains collinear (within numerical accuracy). On the other hand, for the Mn trimer a noncollinear solution is found (Fig. 6) with the nearest neighbors almost antiferromagnetic to each other, but with a collective tilting angle with respect to the substrate. This tilting angle is induced by the ferromagnetic MEI between the central Mn atom with the substrate, competing with the antiferromagnetic MEI with its two companions. The top view of the surface shows that the in-plane components of the magnetic moments are collinear.

The tilting is somewhat smaller $(21.7°)$ for the two Mn atoms with moments up than for the Mn atom with moment down $(28.5°)$. Also the neighboring Ni-surface atoms experience small tilting, with varying angles around $4°-10°$. From the energy point of view, the ground state is the collinear one, $\uparrow\downarrow\uparrow$, with an energy difference of $\Delta E_{\text{Ncol-}\uparrow\downarrow\uparrow}$ $=22.92$ meV with respect to the noncollinear solution.

We have also investigated the cases where the trimers are sitting in the surface layer. No noncollinear solution was found, while there is no change in the collinear ground state which is $\downarrow\uparrow\downarrow$ for the Cr trimer and $\uparrow\downarrow\uparrow$ for Mn trimer.

One should note that the moments of the two first neighboring impurities are almost compensated in the Ferri solution. The third moment determines the total interaction between the substrate and the trimer which has then a net moment coming mainly from the additional impurity. This interaction is identical to the single adatom (or inatom) type of coupling.

TABLE IV. Energy differences between the different calculated collinear magnetic configurations with the $\downarrow\uparrow\downarrow$ configuration. The direction of the arrows represents the direction of the atomic moments relative to the substrate magnetization ($\uparrow$ parallel, $\downarrow$ antiparallel). The middle arrow represents the atom at the right-angle corner of the trimer.

Magn. config.	$\uparrow\uparrow\downarrow$	$\downarrow\uparrow\downarrow$	$\downarrow\downarrow\uparrow$	$\uparrow\downarrow\uparrow$	$\uparrow\uparrow\uparrow$	$\downarrow\downarrow\downarrow$
Cr: $E-E_{\downarrow\uparrow\downarrow}$ (eV)	0.420	0	0.390	0.193		
Mn: $E-E_{\downarrow\uparrow\downarrow}$ (eV)	0.116	0	0.318	-0.184	0.239	0.817

IV. SUMMARY

We have presented a formalism for the treatment of non-collinear magnetic clusters on surfaces and in bulk, based on the Green-function technique of Korringa, Kohn, and Rostoker, and on spin-density-functional theory. We have applied the formalism on the study of small transition-metal clusters (dimers and trimers) on and in the Ni(001) surface.

Emphasis was placed on Cr and Mn clusters, for which we found that magnetic frustration can lead to noncollinear magnetic order. The origin of the frustration is the competition of the antiferromagnetic exchange coupling among the Cr or Mn atoms with the antiferromagnetic (for Cr) or ferromagnetic (for Mn) exchange coupling between the adatoms and the substrate. In this respect, the result is different than the prototype noncollinear configurations arising from antiferromagnetic interactions among atoms in triangular geometry.

We found that Cr and Mn first-neighboring adatom dimers can show noncollinear behavior, while increasing the distance between the adatoms of the dimer leads to the same state as for single adatoms. The energy differences between the collinear ferrimagnetic state and the noncollinear one are $\Delta E_{\text{Ncol-Ferri}}^{\text{Cr}}=39.84$ meV (the ground state is collinear), $\Delta E_{\text{Ncol-Ferri}}^{\text{Mn}}=-13.45$ meV (the ground state is noncollinear). Embedding the dimers in the first surface layer restores the Ferri collinear solution as a ground state also for Mn adatom dimers ($\Delta E_{\text{Ncol-Ferri}}^{\text{Cr}}=24.11$ meV, $\Delta E_{\text{Ncol-Ferri}}^{\text{Mn}}=22.5$ meV).

Our *ab initio* results for dimers are compared to the solution of a classical Heisenberg model with exchange parameters fitted to total-energy calculations. The agreement for the tilting angles in the noncollinear state is good, but the Heisenberg model does not capture the collinear ground state for the Cr dimer. This discrepancy occurs because the Heisenberg model is restricted to constant absolute values of localized spins.

The trimers studied so far are characterized by a collinear ground state: $\downarrow\uparrow\downarrow$ for the Cr trimer and $\uparrow\downarrow\uparrow$ for the Mn trimer. The Mn trimer has also a noncollinear metastable solution with an energy difference $\Delta E_{\text{Ncol-}\uparrow\downarrow\uparrow}=22.92$ meV.

We believe that the energetic proximity of the collinear to the noncollinear states is directly related to the weakness of the exchange interaction with the Ni substrate. Replacing it by an fcc Fe substrate will possibly change the ground state drastically. Work in this direction is in progress and will be reported elsewhere.

---

*Electronic address: s.lounis@fz-juelich.de

†Electronic address: ph.mavropoulos@fz-juelich.de

[1] J. T. Lau, A. Föhlisch, R. Nietubyć, M. Reif, and W. Wurth, Phys. Rev. Lett. **89**, 57201 (2002).

[2] D. M. Eigler and E. K. Schweiser, Nature (London) **344**, 524 (1990).

[3] M. F. Crommie, C. P. Lutz, and D. M. Eigler, Science **262**, 218 (1993).

[4] H. C. Monoharan, C. P. Lutz, and D. M. Eigler, Nature (London) **403**, 512 (2000).

[5] A. Oswald, R. Zeller, and P. H. Dederichs, J. Magn. Magn. Mater. **54-57**, 1247 (1986).

[6] L. M. Sandratskii and P. G. Gulsetskii, J. Phys. F: Met. Phys. **16**, L43 (1986).

[7] J. Kübler, K. H. Höck, and J. Sticht, J. Appl. Phys. **63**, 3482 (1988).

[8] J. Kübler, K. H. Höck, J. Sticht, and A. R. Williams, J. Phys. F: Met. Phys. **18**, 469 (1988).

[9] Y. Tsunoda, J. Phys.: Condens. Matter **1**, 10427 (1989).

[10] Y. Tsunoda, Y. Nishioka, and R. M. Nicklow, J. Magn. Magn. Mater. **128**, 133 (1993).

[11] O. N. Mryasov, A. I. Liechtenstein, L. M. Sandratskii, and V. A. Gubanov, J. Phys.: Condens. Matter **3**, 7683 (1991).

[12] K. Knöpfle, L. M. Sandratskii, and J. Kübler, Phys. Rev. B **62**, 5564 (2000).

[13] Ph. Kurz, F. Förster, L. Nordström, G. Bihlmayer, and S. Blügel, Phys. Rev. B **69**, 24415 (2004).

[14] L. Nordström and D. J. Singh, Phys. Rev. Lett. **76**, 4420 (1996).

[15] E. Sjöstedt and Lars Nordström, Phys. Rev. B **66**, 14447 (2002).

[16] L. M. Sandratskii, Solid State Commun. **75**, 527 (1990).

[17] L. M. Sandratskii, Phys. Rev. B **64**, 134402 (2001).

[18] P. H. Dederichs, S. Blügel, R. Zeller, and H. Akai, Phys. Rev. Lett. **53**, 2512 (1984).

[19] O. Grotheer, C. Ederer, and M. Fähnle, Phys. Rev. B **62**, 5601 (2000).

[20] T. Oda, A. Pasquarello, and R. Car, Phys. Rev. Lett. **80**, 3622 (1998).

[21] D. Hobbs, G. Kresse, and J. Hafner, Phys. Rev. B **62**, 11556 (2000).

[22] C. Kohl and G. F. Bertsch, Phys. Rev. B **60**, 4205 (1999).

[23] N. Papanikolaou, R. Zeller, and P. H. Dederichs, J. Phys.: Condens. Matter **14**, 2799 (2002).

[24] R. Zeller, P. H. Dederichs, B. Ujfalussy, L. Szunyogh, and P. Weinberger, Phys. Rev. B **52**, 8807 (1995); R. Zeller, *ibid.* **55**, 9400 (1997); K. Wildberger, R. Zeller, and P. H. Dederichs, *ibid.* **55**, 10074 (1997).

[25] B. Nonas, K. Wildberger, R. Zeller, and P. H. Dederichs, J. Magn. Magn. Mater. **165**, 137 (1997).

[26] B. Nonas, K. Wildberger, R. Zeller, P. H. Dederichs, and B. L. Gyorffy, Phys. Rev. B **57**, 84 (1998).

[27] B. Nonas, K. Wildberger, R. Zeller, and P. H. Dederichs, Phys. Rev. Lett. **80**, 4574 (1998).

[28] V. Popescu, H. Ebert, B. Nonas, and P. H. Dederichs, Phys. Rev. B **64**, 184407 (2001).

[29] Ph. Mavropoulos, S. Lounis, R. Zeller, and S. Blügel, cond-mat/0411644, Appl. Phys. A: Mater. Sci. Process (to be published).

[30] S. Alexander and P. W. Anderson, Phys. Rev. **133**, A1594 (1964).

[31] A. Oswald, R. Zeller, P. J. Braspenning, and P. H. Dederichs, J. Phys. F: Met. Phys. **15**, 193 (1985).

[32] S. H. Vosko, L. Wilk, and M. Nusair, J. Chem. Phys. **58**, 1200 (1980).

[33] N. Stefanou, H. Akai, and R. Zeller, Comput. Phys. Commun. **60**, 231 (1990); N. Stefanou and R. Zeller, J. Phys.: Condens. Matter **3**, 7599 (1991).

[34] A. I. Liechtenstein, M. I. Katsnelson, V. P. Antropov, and V. A. Gubanov, J. Magn. Magn. Mater. **67**, 65 (1987).